




RESEARCH ARTICLE

 View Article Online
View Journal | View Issue

 Cite this: *Mater. Chem. Front.*,
2023, 7, 6247

Multifunctional dielectric/optical response with broadband white light emission in a hybrid stannic halide crystal†

 Qing-Feng Luo, Hao-Fei Ni, Pei-Zhi Huang, Ming Zhu, Chang-Feng Wang,
Qian-Hao Zhuo, Da-Wei Fu, * Yi Zhang * and Zhi-Xu Zhang *

The integration of switchable dielectrics and luminescent properties has significant application potential in emerging sensing and optoelectronic devices. Despite great progress in various colours, such as green, red, or yellow lights, the dielectric switching response equipped with intrinsic broadband white-light emission in a single material has been a very rare and ongoing challenge. Herein, we present an organic–inorganic hybrid crystal (TPMA)₂SnCl₆ (TPMA = 3-methoxypropylamine), which simultaneously exhibits a dual-channel electric/optical response with switchable dielectric biostability and broadband white light emission. This is a rare phenomenon among the reported switchable dielectric materials. Additionally, its analogue (TPMA)₂SnBr₆ displays a thermochromic phenomenon related to temperature-dependent [SnBr₆] octahedral distortion. This study would provide constructive insights for exploring the integration of dual-channel optical/electrical response characteristics in a single material at the molecular level.

 Received 17th July 2023,
Accepted 2nd October 2023

DOI: 10.1039/d3qm00800b

rsc.li/frontiers-materials

Introduction

The integration of multiple physical properties into a single material for multifunctional applications has long been a pursued objective for better application selectivity, freedom and possible superimposed coupling effects.^{1–6} As stimulus-responsive materials, switchable dielectrics exhibit a reversible transition between low and high states in dielectric permittivity, holding great promise for use in temperature-control switches and sensing devices.^{7–13} Accompanied by thermally driven structural phase transitions, the electric polarization response of switchable dielectrics under an electric field changes reversibly, reflecting the high contrast switching of the dielectric constant.^{14–19} This switching response of the electrical channel, in combination with other functions, enables the exploration of more possibilities, including fascinating physical phenomena and exotic effects.^{20–23} In particular, luminescent dielectric switches have aroused great interest because they offer great potential in novel optoelectronic applications with switching

fluorescence imaging, multi-level control and sensing.^{24–27} Among them, white-light-emitting materials, as an attractive solution for the disadvantages of traditional incandescent and fluorescent lighting sources, are highly desired and have rarely been reported so far.²⁸ Inorganic materials have been the mainstream of research and applications of switchable dielectrics with various functions owing to their excellent performance and chemical stability with widespread recognition.²⁹ The preparation of luminescent dielectric switches in inorganic materials often involves doping additional elements, such as rare earth metals, into multi-component products with possible troubles of high-temperature sintering and phase separation.^{30,31} The implementation of luminescent dielectric switches in a single homogeneous material has always been an ongoing scientific task, while one with white-light is more challenging.

In molecular systems, organic–inorganic hybrid materials (OIHMs) possess a vast chemical diversity, structural adaptability, and easy preparation that has garnered increasing attention as a beneficial supplement to inorganic materials.^{32–35} The presence of organic components in the construction of hybrid materials renders them susceptible to order–disorder phase transitions under thermal stimuli, resulting in dielectric anomalies. Simultaneously, the inorganic metal fraction induces many other fascinating physicochemical properties, such as photoluminescence.^{36–38} For example, our group has reported a dielectric responsive OIHMs (pyrrolidinium)MnX₃ (X = Cl, Br), exhibiting a strong red-light emission attributed to the inorganic anion octahedron of

Institute for Science and Applications of Molecular Ferroelectrics, Key Laboratory of the Ministry of Education for Advanced Catalysis Materials, Zhejiang Normal University, Jinhua, 321004, People's Republic of China. E-mail: dawei@zjnu.edu.cn, yizhang1980@seu.edu.cn, zhangzhixu@zjnu.edu.cn

† Electronic supplementary information (ESI) available: Experimental section, Fig. S1–S12, Tables S1–S8. CCDC 2174141, 2174142 and 2242964. For ESI and crystallographic data in CIF or other electronic format see DOI: <https://doi.org/10.1039/d3qm00800b>

[MnX_6].^{39,40} Subsequently, many dielectric multifunctional materials emitting various colors, such as red, green, yellow, blue, and others, were explored, significantly enriching the development of fluorescent dielectric multifunctional materials.^{38,41–45} Luo *et al.* also reported white light dielectric responsive lead-based materials, which have a warm white light a color temperature of 4423 K and have high color rendering index (CRI) of up to 86.²⁸ Despite these great advances, the single material simultaneously equipped with a dual channel optical/electrical response of dielectric switching response and intrinsic broadband white-light emission has been very rare and an ongoing challenge.

Herein, we successfully achieved the integration of the dielectric response and luminescent properties in a single material $(\text{TMPA})_2\text{SnCl}_6$ (TMPA = 3-methoxypropylamine). With temperature-dependent structural phase transition, it shows a clear dielectric switching response with good reversibility between low and high states. The phase transition has a large entropy change of $69.3 \text{ J mol}^{-1} \text{ K}^{-1}$, which is higher than that of the vast majority of reported dielectric switching responsive materials, showing potential in storing thermal energy and cooling. More remarkably, $(\text{TMPA})_2\text{SnCl}_6$ possesses luminescent properties for which it emits fascinating broadband white light with a long lifetime of $6.382 \mu\text{s}$. Its analogue $(\text{TMPA})_2\text{SnBr}_6$ shows obvious thermochromic properties in combination with dielectric switching. This work may offer a fresh perspective on the effective design and tuning integration of the multifunctional properties of white light dielectric multifunctional materials.

Experimental section

Synthetic procedures

Without further purification, all chemical reagents used herein are purchased directly from commercial suppliers. 3-Methoxypropylamine (TMPA, 98%, Meryer-Shanghai), Tin(IV) chloride (SnCl_4 , 99%, Meryer-Shanghai), Tin(IV) bromide (SnBr_4 , 98%, Meryer-Shanghai), Polymethylmethacrylate ($(\text{C}_5\text{H}_8\text{O}_2)_n$, AR, Meryer-Shanghai), Dichloromethane (CH_2Cl_2 , 99.5%, Meryer-Shanghai), Ethanol ($\text{CH}_3\text{CH}_2\text{OH}$, 99%, Meryer-Shanghai) hydrochloric acid (HCl, AR, GuoYao-Jinghua) and Hydrobromic acid (HBr, AR, Meryer-Shanghai).

Synthesis of $(\text{TMPA})_2\text{SnCl}_6$

Prepare a cup of a mixed solution of concentrated hydrochloric acid and water (1:4) with a total of 20 mL. Then, 3-methoxypropylamine (6 mmol, 0.535 g) and Tin(IV) chloride (3 mmol, 0.781 g) were added to the prepared solution and stirred for 30 minutes. By slow evaporation at room temperature, colourless and transparent block crystals of $(\text{TMPA})_2\text{SnCl}_6$ were obtained after three days.

Synthesis of $(\text{TMPA})_2\text{SnBr}_6$

Prepare one cup of a mixed solution of hydrobromic acid and ethanol (1:1) with a total of 20 mL. Then, 3-Methoxypropylamine (6 mmol, 0.535 g) and Tin(IV) bromide (3 mmol, 1.314 g) were added to the prepared solution and stirred for 30 minutes.

By slow evaporation at room temperature, pale yellow and transparent block crystals of $(\text{TMPA})_2\text{SnBr}_6$ were obtained after one week.

Fabricate a white LED lamp

First, a cup of dichloromethane solution was prepared with 10 mL. Subsequently, polymethylmethacrylate (PMMA, 1 g) was added to the prepared solution and sonicated for 2 hours to complete dissolution. Then, $(\text{TMPA})_2\text{SnCl}_6$ (0.5 g) was added to the mixed solution and stirred for 30 minutes. Finally, the mixed solution was directly coated with a commercial ultraviolet LED lamp (365 nm) and evaporated in the air atmosphere for 24 hours to obtain a white LED lamp.

Measurement methods

The crystal structure and characteristics of this paper were determined by X-ray single crystal diffraction (SC-XRD), the differential scanning calorimetry (DSC) instrument, dielectric measurement, thermogravimetric analysis, powder X-ray diffraction, UV-Vis measurements and fluorescence spectrofluorometer. All the details are presented in the ESI.†

Results and discussion

Thermodynamic analysis of phase transition behaviours

The compounds $(\text{TMPA})_2\text{SnCl}_6$ and $(\text{TMPA})_2\text{SnBr}_6$ are obtained through evaporative crystallization (Fig. 1a). The simulated crystal morphology of $(\text{TMPA})_2\text{SnCl}_6$ is basically consistent with the actual one (Fig. 1b). To investigate the phase transition behaviors of the two compounds, differential scanning calorimetry (DSC) detection was performed. For $(\text{TMPA})_2\text{SnCl}_6$, Fig. 1c illustrates a pair of reversible endothermic/exothermic peaks at 391.3/328.9 K during the heating/cooling process with a wide thermal hysteresis of 62.4 K, characterizing first-order phase transitions. Utilizing DSC data, the entropy variation (ΔS)

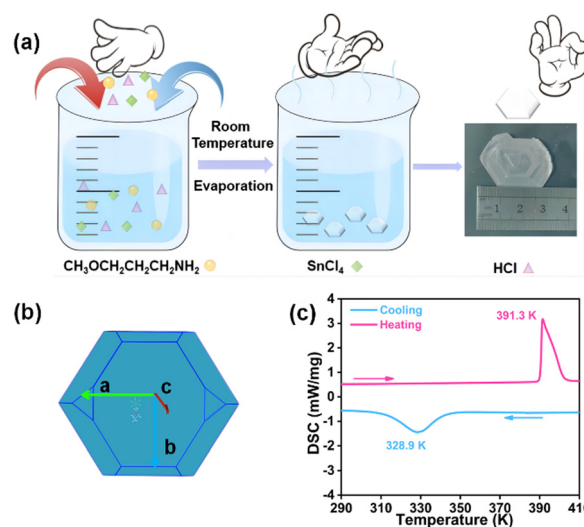


Fig. 1 (a) The synthesis of $(\text{TMPA})_2\text{SnCl}_6$. (b) $(\text{TMPA})_2\text{SnCl}_6$ crystal simulation diagram. (c) DSC curve of $(\text{TMPA})_2\text{SnCl}_6$ in heating-cooling runs.

is determined to be $75.45 \text{ J mol}^{-1} \text{ K}^{-1}$ using the formula $\Delta S = \Delta H/T$, as detailed in the ESI†. This material with a significant change in entropy holds the potential to serve as a promising candidate for energy storage.^{46,47} For $(\text{TMPA})_2\text{SnBr}_6$, the reversible phase transition temperatures are 374.7/361.3 K, and the value of ΔS is calculated to be $49.90 \text{ J mol}^{-1} \text{ K}^{-1}$ (Fig. S1, ESI†). Surprisingly, $(\text{TMPA})_2\text{SnBr}_6$ exhibits a switchable thermochromic response, which may be attributed to the distortion of inorganic skeleton octahedra due to the Jahn–Teller effect (Fig. S2 and S3, ESI†).^{26,48} Furthermore, thermogravimetric analysis (TGA) was conducted to demonstrate the thermal stability of both compounds. The TGA curves reveal that the decomposition temperatures for $(\text{TMPA})_2\text{SnCl}_6$ and $(\text{TMPA})_2\text{SnBr}_6$ are 516 K and 505 K, respectively (Fig. S4, ESI†), surpassing their phase transition temperatures. For convenience, the phases below and above the phase transition temperature in the heating run were labeled as the low-temperature phase (LTP) and high-temperature phase (HTP), respectively.

Structural and intermolecular interaction analyses

The mechanism of reversible phase transitions is revealed through variable-temperature single-crystal X-ray diffraction. At LTP, both $(\text{TMPA})_2\text{SnCl}_6$ and $(\text{TMPA})_2\text{SnBr}_6$ are crystallized in space group *Pbca* in orthorhombic point group *mmm*, showing a zero-dimensional structure, where the cations are in the cavities of the octahedron (Table S1 and Fig. S5, ESI†). As shown in Table S1 (ESI†), the cell parameters of the two compounds are similar, while $(\text{TMPA})_2\text{SnBr}_6$ exhibits a larger cell volume than $(\text{TMPA})_2\text{SnCl}_6$. The asymmetric units of $(\text{TMPA})_2\text{SnX}_6$ ($X = \text{Cl}, \text{Br}$) comprise half of an inorganic octahedron [SnX_6] and an organic amine cation (Fig. S6, ESI†). For inorganic skeleton, it is composed of a well-organized arrangement of octahedrons, coordinated by one Sn ion and six Cl ions, in which the bond length of Sn–Cl is between 2.4200 and 2.4566 Å and the bond angle of Cl–Sn–Cl varies from 88.24 to 91.75° (Table S2, ESI†). At HTP, $(\text{TMPA})_2\text{SnBr}_6$ belonged to the *Pnma* space group in the orthorhombic *mmm* point group, while the detailed structural information for $(\text{TMPA})_2\text{SnCl}_6$ could not be obtained *via* single-crystal X-ray diffraction owing to poor crystal quality at high temperatures (Table S1, ESI†). Hence, variable-temperature powder X-ray diffraction was conducted to investigate the structural alterations of $(\text{TMPA})_2\text{SnCl}_6$ (Fig. S7a, ESI†). As depicted in Fig. S7a (ESI†), it is evident that the symmetry of $(\text{TMPA})_2\text{SnCl}_6$ gradually increases and that the diffraction peaks undergo significant changes as the temperature increases, providing evidence for a structural transition occurring in $(\text{TMPA})_2\text{SnCl}_6$. Using Pawley refinement, it was subsequently determined that the space group of $(\text{TMPA})_2\text{SnCl}_6$ at HTP is likely *Pcmm*, which is a non-standard space group derived from the *Pnma* space group (Fig. S7b and c, ESI†). Coincidentally, it is identical to that of $(\text{TMPA})_2\text{SnBr}_6$ at HTP. In fact, it is reasonable that $(\text{TMPA})_2\text{SnCl}_6$ and $(\text{TMPA})_2\text{SnBr}_6$ are in the same space group after undergoing phase transition because of the similar stacking models of the two compounds at LTP.

Therefore, analysing the structural transition of $(\text{TMPA})_2\text{SnBr}_6$ from low to high temperatures can provide insights into the

corresponding transformation in $(\text{TMPA})_2\text{SnCl}_6$. $(\text{TMPA})_2\text{SnBr}_6$ displays two distinct types of hydrogen bonding, namely intramolecular hydrogen bonding within the amine itself and intermolecular hydrogen bonding between the amine and bromine atoms in the inorganic framework (Fig. S5 and S8, ESI†). For intramolecular hydrogen bonding, as shown in Fig. S8 (ESI†), the distance at HTP is 2.372 Å, which is larger than that at LTP (2.033 Å), indicating a reduction in the intramolecular hydrogen bonding force after the phase transition. Similarly, in the case of intermolecular hydrogen bonding, the N–H...Br hydrogen bonding distance ranges from 2.71 to 2.88 Å in the LTP and between 2.72 and 3.08 Å in the HTP, implying a significant decrease in intermolecular hydrogen bonding force during phase transition (Tables S5 and S6, ESI†). According to the single-crystal X-ray diffraction data, the cations undergo an order–disorder transformation, resulting in the weakening of the hydrogen bond strength, which in turn enhances the likelihood of atomic vibration at high temperatures (Fig. 2a–c and Fig. S1, ESI†).

Notably, the phase transition temperature of $(\text{TMPA})_2\text{SnCl}_6$ surpasses that of $(\text{TMPA})_2\text{SnBr}_6$, which can be explained by the structural disparities between them. This phenomenon may be attributed to the steric effect within a unit cell. The cell volume of $(\text{TMPA})_2\text{SnBr}_6$ is significantly larger than $(\text{TMPA})_2\text{SnCl}_6$, indicating that the steric effect of $(\text{TMPA})_2\text{SnCl}_6$ is stronger (Fig. 2d and e). For both intramolecular and intermolecular hydrogen bondings, the hydrogen bond distance of $(\text{TMPA})_2\text{SnCl}_6$ is shorter than that of $(\text{TMPA})_2\text{SnBr}_6$ (Fig. S5a and b, ESI†), meaning that organic cations establish a higher energy barrier in $(\text{TMPA})_2\text{SnCl}_6$. Consequently, more energy is required for the steric effect, resulting in a higher phase transition temperature for $(\text{TMPA})_2\text{SnCl}_6$. In addition, the void volume was 1924.6 and 2067 Å³, and the volumes of the octahedral cavities for $(\text{TMPA})_2\text{SnCl}_6$ and $(\text{TMPA})_2\text{SnBr}_6$ were calculated to be 19.3 and 23.4 Å³, respectively (Table S7, ESI†). The cationic amine in $(\text{TMPA})_2\text{SnCl}_6$ exhibits a greater steric hindrance, which breaks through a higher energy

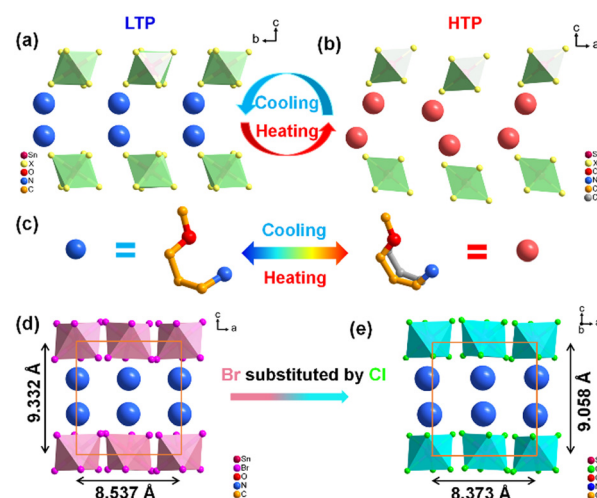


Fig. 2 (a) Molecular structure of $(\text{TMPA})_2\text{SnX}_6$ ($X = \text{Cl}, \text{Br}$) at 300 K. (b) Molecular structure of $(\text{TMPA})_2\text{SnX}_6$ ($X = \text{Cl}, \text{Br}$) at 380 K. (c) Diagram of ordered and disordered about TMPA. (d) Packing structures of $(\text{TMPA})_2\text{SnCl}_6$ at 300 K. (e) Packing structures of $(\text{TMPA})_2\text{SnBr}_6$ at 300 K.

barrier during phase transformation, thereby leading to a higher phase transition temperature for $(\text{TMPA})_2\text{SnCl}_6$. Moreover, powder X-ray diffraction analysis was conducted on $(\text{TMPA})_2\text{SnCl}_6$ and $(\text{TMPA})_2\text{SnBr}_6$ (Fig. S9a and b, ESI[†]). The high agreement between the experimental values and simulation results provides credible evidence for the phase purity of the crystals. We performed powder PXRD measurement experiments on samples kept in an air atmosphere for 1 week, 2 weeks and 6 months. The positions of the diffraction peaks of the samples stored at different times remained consistent, indicating that the samples had good stability (Fig. S10, ESI[†]).

Photoluminescence properties

$(\text{TMPA})_2\text{SnCl}_6$ exhibits photoluminescence (PL) and emits white light. As shown in Fig. 3a, both the powder and centimetre-level crystals of $(\text{TMPA})_2\text{SnCl}_6$ display a white appearance when exposed to natural light. Remarkably, $(\text{TMPA})_2\text{SnCl}_6$ exhibits uncommon white luminescence under commercial UV irradiation (365 nm), which is exceedingly rare among organic-inorganic hybrid phase transition materials. The luminescence properties of $(\text{TMPA})_2\text{SnCl}_6$ were further investigated through UV absorption spectroscopy and solid-state PL emission spectroscopy analysis. The ultraviolet absorption spectrum exhibits a tiny absorption peak at approximately 330 nm, signifying that the excitation peak of $(\text{TMPA})_2\text{SnCl}_6$ is close to this wavelength (Fig. 3b). Expectedly, the excitation wavelength of $(\text{TMPA})_2\text{SnCl}_6$ was obtained at 337 nm, and the maximum emission peak of broadband light was observed at 527 nm with a large Stokes shift of 190 nm (Fig. S9, ESI[†]). Based on the average lifetime obtained from $\tau_{\text{ave}} = \tau_1 a_1 + \tau_2 a_2$, the average decay lifetime (τ_{ave}) of the emitted light was calculated to be 6.382 μs for $(\text{TMPA})_2\text{SnCl}_6$ (Fig. 3c). $(\text{TMPA})_2\text{SnCl}_6$ (0.31, 0.35) is a high-quality pure white light material that closely matches the standard pure white light colour coordinates (0.33, 0.33), as determined by the International Committee on Electronic Analysis (CIE) (Fig. 3d). The broadband white light emission of tin bromide, characterized

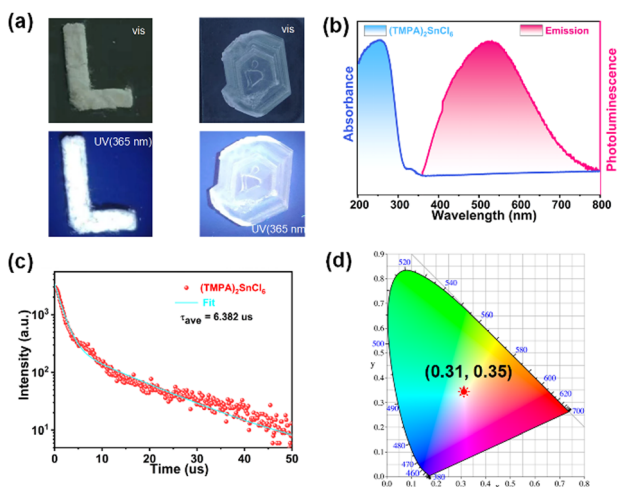


Fig. 3 (a) Crystal and powder of $(\text{TMPA})_2\text{SnCl}_6$ emit light at 365 nm. (b) Absorption and emission spectra of $(\text{TMPA})_2\text{SnCl}_6$. (c) Luminous lifetime of $(\text{TMPA})_2\text{SnCl}_6$. (d) CIE chromaticity coordinates of $(\text{TMPA})_2\text{SnCl}_6$.

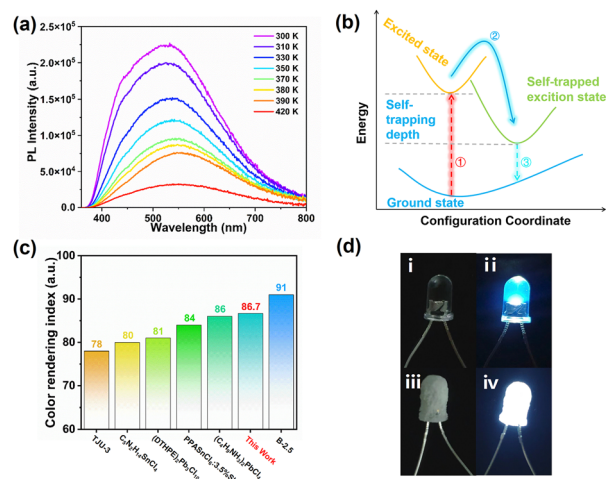


Fig. 4 (a) Temperature-dependent emission spectra of $(\text{TMPA})_2\text{SnCl}_6$ at the excitation of 337 nm. (b) Diagram of PL mechanism in $(\text{TMPA})_2\text{SnCl}_6$. (c) A color rendering index of $(\text{TMPA})_2\text{SnCl}_6$ compared with tin/lead-based materials. (d) Photographs of LEDs (i) commercial UV-LED and (ii) commercial UV-LED lamps illuminate light (365 nm); the same UV-LED coated with $(\text{TMPA})_2\text{SnCl}_6$ in the states of turned off (iii) and on (iv).

by a large Stokes shift (190 nm), may be attributed to self-trapped excitons (STEs), which are induced by structural distortions in the octahedral excited state of $[\text{SnCl}_6]^{2-}$ (Fig. 3b and Fig. S11, ESI[†]).^{49,50}

To further clarify the broadband emission mechanism, we measure temperature-dependent emission spectra of $(\text{TMPA})_2\text{SnCl}_6$ at the excitation of 337 nm. It is obvious that the PL intensity of $(\text{TMPA})_2\text{SnCl}_6$ slowly decreases as the temperature increases. An increase in test temperature results in an increase in the nonradiative transitions, thereby weakening the PL (Fig. 4a). The broad emission of the bulk crystal weakened and increased with increasing temperature, indicating that the white-light emission of $(\text{TMPA})_2\text{SnCl}_6$ is attributed to STEs (Fig. 4a). Moreover, the quantum yield of $(\text{TMPA})_2\text{SnCl}_6$ was measured to be 3.88%. $(\text{TMPA})_2\text{SnCl}_6$ is warm white light with a correlated color temperature of (CCT) 5390 K and a high color render index (CRI) of up to 86.7. It is higher than the classical white photoluminescence source (CRI \approx 65). The CRI of $(\text{TMPA})_2\text{SnCl}_6$ is remarkably higher than that of most tin/lead materials and exhibits excellent color rendering capacity (Fig. 4c and Table S8, ESI[†]).^{28,51–55} To show the practicality of the material, $(\text{TMPA})_2\text{SnCl}_6$ is evenly coated with commercial LED light (365 nm), which emits bright white light (Fig. 4d). Thus, $(\text{TMPA})_2\text{SnCl}_6$ possesses potential as a solid-state broadband white light emitter.

Dielectric analysis

The reversible phase transition induced by temperature often leads to significant dielectric anomalies. Temperature-dependent permittivity measurements were performed to further substantiate the reversible phase transitions of the two compounds and to investigate their dielectric characteristics. As illustrated in Fig. 4a, the dielectric response of $(\text{TMPA})_2\text{SnCl}_6$ exhibits a pair of anomalous changes at approximately 390/330 K, with the dielectric

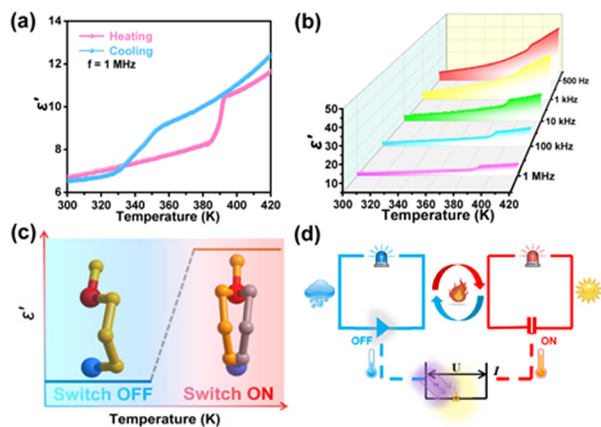


Fig. 5 (a) Dielectric constant of $(\text{TMPA})_2\text{SnCl}_6$. (b) Temperature dependence of the real part (ϵ') of $(\text{TMPA})_2\text{SnCl}_6$ at different frequencies in the heating run. (c) Scheme of the dielectric switch with a bistable state. (d) Simulated application of the optical/thermal integrated multifunctional switch sensor.

constant transitioning from 6 to 10. For $(\text{TMPA})_2\text{SnBr}_6$, the dielectric anomalies occurring near 370 K also demonstrate a phase transition (Fig. S12a, ESI[†]). Moreover, the dielectric constant exhibits a decreasing trend with increasing frequency, indicating that the dielectric constant of the two compounds is not only temperature sensitive but also frequency dependent (Fig. S12b, ESI[†]). A dielectric phenomenon refers to the polarization of a dielectric material under the influence of an applied voltage, which can be classified into four types: electronic displacement polarization, ionic displacement polarization, orientational polarization and space charge polarization. At higher frequencies, the electron polarization exhibits an immediate response to changes in the electric field, while the dipole orientation polarization does not exhibit instantaneous matching, thereby causing electric polarization dependence on frequency. A high dielectric constant state at a high temperature means “ON”, and a low dielectric constant state at a low temperature means “OFF” (Fig. 5c). When the temperature of the environment is higher than the phase transition temperature, the dielectric switch connects “ON”. The alarm is automatically turned off when the ambient temperature falls below the phase transition temperature (Fig. 5d). Moreover, the combination of the dielectric switching property and white light emission property of $(\text{TMPA})_2\text{SnCl}_6$ renders it a promising candidate for employment as a luminescent sensor.

Conclusions

In summary, we report the dual-channel electric/optical response with switchable dielectric biostability and broadband white light emission in an organic–inorganic hybrid crystal $(\text{TMPA})_2\text{SnCl}_6$. Its analogue $(\text{TMPA})_2\text{SnBr}_6$ displays a thermochromic phenomenon that is related to temperature-dependent $[\text{SnBr}_6]$ octahedral distortion in combination with a dielectric switching response. Both of them experience cationic order–disorder type phase transitions at 391.3 K and 374.3 K, respectively. The higher phase transition temperature of the former is attributed to the steric

effect, which constrains the dynamic motion of cations. Strikingly, $(\text{TMPA})_2\text{SnCl}_6$ emits fascinating broadband white light with a long lifetime of 6.382 μs and a high CRI of up to 86.7, which are higher than those of most organic–inorganic hybrid crystals. Our finding provides an attractive case to enrich the white light emitting material and would facilitate the development of a multi-channel electric/optical response toward more possibilities for new optoelectronics.

Author contributions

Q.-F. L., D.-W. F. and Z.-X. Z. conceived and designed the experiments. Q.-F. L. and P.-Z. H. prepared the samples and wrote the paper. H.-F. N. and Y. Z. performed the single crystal measurement and analysis. P.-Z. H., M. Z., Q.-H. Z. contributed to DSC, dielectric measurements. Z.-X. Z. and C.-F. W. contributed to the analysis of photoluminescence. D.-W. F., Y. Z. and Z.-X. Z. supervised the project. All the authors discussed the results and commented on the manuscript.

Conflicts of interest

There are no conflicts to declare.

Acknowledgements

This work was financially supported by the Natural Science Foundation of Zhejiang Province (LZ20B010001) and the National Natural Science Foundation of China (grant 21991141).

Notes and references

- B. Saporov and D. B. Mitzi, Organic-Inorganic Perovskites: Structural Versatility for Functional Materials Design, *Chem. Rev.*, 2016, **116**, 4558–4596.
- F.-F. Di, H. Peng, H. Zhang, X.-Q. Huang, W.-J. Chen, Y.-L. Liu and Y.-Y. Tang, Monofluorine substitution achieved high-Tc dielectric transition in a one-dimensional lead bromide hybrid photoluminescent perovskite semiconductor, *Mater. Chem. Front.*, 2021, **5**, 2842–2848.
- S. Parola, B. Julián-López, L. D. Carlos and C. Sanchez, Optical Properties of Hybrid Organic-Inorganic Materials and their Applications, *Adv. Funct. Mater.*, 2016, **26**, 6506–6544.
- R. G. Xiong, S. Q. Lu, Z. X. Zhang, H. Cheng, P. F. Li and W. Q. Liao, A Chiral Thermochromic Ferroelastic with Seven Physical Channel Switches, *Angew. Chem., Int. Ed.*, 2020, **59**, 9574–9578.
- D.-W. Fu, H.-L. Cai, Y. Liu, Q. Ye, W. Zhang, Y. Zhang, X.-Y. Chen, G. Giovannetti, M. Capone, J. Li and R.-G. Xiong, Diisopropylammonium Bromide Is a High-Temperature Molecular Ferroelectric Crystal, *Science*, 2013, **339**, 425–428.
- J. F. Scott, Applications of Modern Ferroelectrics, *Science*, 2007, **315**, 954–959.
- H. Peng, Y.-H. Liu, X.-Q. Huang, Q. Liu, Z.-H. Yu, Z.-X. Wang and W.-Q. Liao, Homochiral one-dimensional ABX₃ lead

- halide perovskites with high-Tc quadratic nonlinear optical and dielectric switchings, *Mater. Chem. Front.*, 2021, **5**, 4756–4763.
- 8 Z. Sun, Y. Tang, S. Zhang, C. Ji, T. Chen and J. Luo, Ultrahigh Pyroelectric Figures of Merit Associated with Distinct Bistable Dielectric Phase Transition in a New Molecular Compound: Di-n-Butylammonium Trifluoroacetate, *Adv. Mater.*, 2015, **27**, 4795–4801.
 - 9 Z.-Y. Du, T.-T. Xu, B. Huang, Y.-J. Su, W. Xue, C.-T. He, W.-X. Zhang and X.-M. Chen, Switchable Guest Molecular Dynamics in a Perovskite-Like Coordination Polymer toward Sensitive Thermoresponsive Dielectric Materials, *Angew. Chem., Int. Ed.*, 2015, **54**, 914–918.
 - 10 M. Matsuki, T. Yamada, N. Yasuda, S. Dekura, H. Kitagawa and N. Kimizuka, Nonpolar-to-Polar Phase Transition of a Chiral Ionic Plastic Crystal and Switch of the Rotation Symmetry, *J. Am. Chem. Soc.*, 2018, **140**, 291–297.
 - 11 H.-Y. Ye, Y.-Y. Tang, P.-F. Li, W.-Q. Liao, J.-X. Gao, X.-N. Hua, H. Cai, P.-P. Shi, Y.-M. You and R.-G. Xiong, Metal-free three-dimensional perovskite ferroelectrics, *Science*, 2018, **361**, 151–155.
 - 12 R. Shang, Z.-M. Wang and S. Gao, A 36-Fold Multiple Unit Cell and Switchable Anisotropic Dielectric Responses in an Ammonium Magnesium Formate Framework, *Angew. Chem., Int. Ed.*, 2015, **54**, 2534–2537.
 - 13 S. Furukawa, J. Wu, M. Koyama, K. Hayashi, N. Hoshino, T. Takeda, Y. Suzuki, J. Kawamata, M. Saito and T. Akutagawa, Ferroelectric columnar assemblies from the bowl-to-bowl inversion of aromatic cores, *Nat. Commun.*, 2021, **12**, 768.
 - 14 Z.-Y. Du, T.-T. Xu, B. Huang, Y.-J. Su, W. Xue, C.-T. He, W.-X. Zhang and X.-M. Chen, Switchable Guest Molecular Dynamics in a Perovskite-Like Coordination Polymer toward Sensitive Thermoresponsive Dielectric Materials, *Angew. Chem., Int. Ed.*, 2015, **54**, 914–918.
 - 15 C. Shi, X. Zhang, Y. Cai, Y.-F. Yao and W. Zhang, A Chemically Triggered and Thermally Switched Dielectric Constant Transition in a Metal Cyanide Based Crystal, *Angew. Chem., Int. Ed.*, 2015, **54**, 6206–6210.
 - 16 J.-P. Zhao, J. Xu, S.-D. Han, Q.-L. Wang and X.-H. Bu, A Niccolite Structural Multiferroic Metal–Organic Framework Possessing Four Different Types of Bistability in Response to Dielectric and Magnetic Modulation, *Adv. Mater.*, 2017, **29**, 1606966.
 - 17 W. Zhang, H.-Y. Ye, R. Graf, H. W. Spiess, Y.-F. Yao, R.-Q. Zhu and R.-G. Xiong, Tunable and Switchable Dielectric Constant in an Amphidynamic Crystal, *J. Am. Chem. Soc.*, 2013, **135**, 5230–5233.
 - 18 J. Ma, Q. Xu, L. Ye, Q. Wang, Z. Gong, C. Shi, H. Ye and Y. Zhang, Structural phase transition and dielectric switching in an organic-inorganic hybrid rare-earth double perovskite-type compound: $(\text{DMP})_2\text{LaRb}(\text{NO}_3)_6$ (DMP = *N,N*-dimethylpyrrolidinium cation), *J. Rare Earths*, 2022, **40**, 937–941.
 - 19 Y. Yu, P. Huang, Y. Wang, Z. Zhang, T. Zhang, Y. Zhang and D. Fu, X-site doping in ABX₃ triggers phase transition and higher T_c of the dielectric switch in perovskite, *Chin. Chem. Lett.*, 2021, **32**, 3558–3561.
 - 20 Y. L. Zeng, X. Q. Huang, C. R. Huang, H. Zhang, F. Wang and Z. X. Wang, Unprecedented 2D Homochiral Hybrid Lead-Iodide Perovskite Thermochromic Ferroelectrics with Ferroelastic Switching, *Angew. Chem., Int. Ed.*, 2021, **60**, 10730–10735.
 - 21 L. Zhou, P.-P. Shi, X.-M. Liu, J.-C. Feng, Q. Ye, Y.-F. Yao, D.-W. Fu, P.-F. Li, Y.-M. You, Y. Zhang and R.-G. Xiong, An above-room-temperature phosphonium-based molecular ferroelectric perovskite, $[(\text{CH}_3)_4\text{P}]\text{CdCl}_3$, with Sb³⁺-doped luminescence, *NPG Asia Mater.*, 2019, **11**, 15.
 - 22 X. Hu, H. Xu, W. Guo, S. Han, Y. Liu, Y. Ma, Q. Fan, J. Luo and Z. Sun, $[\text{C}_5\text{H}_{12}\text{N}]_2\text{SnBr}_6$: a lead-free phase transition compound with switchable quadratic nonlinear optical properties, *Mater. Chem. Front.*, 2023, **7**, 1599–1606.
 - 23 Y.-F. Gao, Z.-X. Zhang, T. Zhang, C.-Y. Su, W.-Y. Zhang and D.-W. Fu, Regulated molecular rotor in phase transition materials with switchable dielectric and SHG effect, *Mater. Chem. Front.*, 2020, **4**, 3003–3012.
 - 24 Z.-X. Zhang, C.-Y. Su, J.-X. Gao, T. Zhang and D.-W. Fu, Mechanochemistry enables optical-electrical multifunctional response and tunability in two-dimensional hybrid perovskites, *Sci. China Mater.*, 2020, **64**, 706–716.
 - 25 H. Peng, H. Cheng, Y.-H. Liu, M.-J. Yang, W.-Q. Liao and Y. Ai, Enantiomeric perovskite with a dual phase transition at high temperature, *J. Mater. Chem. C*, 2021, **9**, 1918–1922.
 - 26 G. Teri, H.-F. Ni, Q.-F. Luo, X.-P. Wang, J.-Q. Wang, D.-W. Fu and Q. Guo, Tin-based organic–inorganic metal halides with a reversible phase transition and thermochromic response, *Mater. Chem. Front.*, 2023, **7**, 2235–2240.
 - 27 Y. Zeng, J. Liu, L. Zhou, X. Deng, W. Yang, X. Yan, Y. Luo, X. Zhu, X. Huang, X. Song and Y. Tang, An organic-inorganic hybrid thermochromic ferroelastic with multi-channel switches, *Chin. Chem. Lett.*, 2023, **34**, 108127.
 - 28 C. Ji, S. Wang, L. Li, Z. Sun, M. Hong and J. Luo, The First 2D Hybrid Perovskite Ferroelectric Showing Broadband White-Light Emission with High Color Rendering Index, *Adv. Funct. Mater.*, 2018, **29**, 1805038.
 - 29 K. J. Choi, M. Biegalski, Y. L. Li, A. Sharan, J. Schubert, R. Uecker, P. Reiche, Y. B. Chen, X. Q. Pan, V. Gopalan, L. Q. Chen, D. G. Schlom and C. B. Eom, Enhancement of Ferroelectricity in Strained BaTiO₃ Thin Films, *Science*, 2004, **306**, 1005–1009.
 - 30 X. Yang, Z. Shao and H. Ru, Preparation and Characterisation of Sr₂CeO₄:Eu³⁺ Rare Earth Luminescent Material by High Temperature Mechano-Chemical Method, *J. Mater. Sci. Technol.*, 2016, **32**, 1066–1070.
 - 31 J. Xiao, W. Zhang, T. Wang, J. Zhang and H. Du, Photoluminescence enhancement in a Na₅Y(MoO₄)₄:Dy³⁺ white-emitting phosphor by partial replacement of MoO₄²⁻ with WO₄²⁻ or VO₄³⁻, *Ceram. Int.*, 2021, **47**, 12028–12037.
 - 32 X.-G. Chen, X.-J. Song, Z.-X. Zhang, P.-F. Li, J.-Z. Ge, Y.-Y. Tang, J.-X. Gao, W.-Y. Zhang, D.-W. Fu, Y.-M. You and R.-G. Xiong, Two-Dimensional Layered Perovskite Ferroelectric with Giant Piezoelectric Voltage Coefficient, *J. Am. Chem. Soc.*, 2020, **142**, 1077–1082.
 - 33 C.-Y. Su, Z.-X. Zhang, W.-Y. Zhang, P.-P. Shi, D.-W. Fu and Q. Ye, Unique Design Strategy for Dual Phase Transition

- That Successfully Validates Dual Switch Implementation in the Dielectric Material, *Inorg. Chem.*, 2020, **59**, 4720–4728.
- 34 T. Shao, R.-Y. Ren, P.-Z. Huang, H.-F. Ni, C.-Y. Su, D.-W. Fu, L.-Y. Xie and H.-F. Lu, Metal ion modulation triggers dielectric double switching and green fluorescence in A_2MX_4 -type compounds, *Dalton Trans.*, 2022, **51**, 2005–2011.
- 35 C. Y. Su, Y. F. Yao, Z. X. Zhang, Y. Wang, M. Chen, P. Z. Huang, Y. Zhang, W. C. Qiao and D. W. Fu, The construction of a two-dimensional organic-inorganic hybrid double perovskite ferroelastic with a high T_c and narrow band gap, *Chem. Sci.*, 2022, **13**, 4794–4800.
- 36 Y.-P. Gong, X.-X. Chen, G.-Z. Huang, W.-X. Zhang and X.-M. Chen, Ferroelasticity, thermochromism, semi-conductivity, and ferromagnetism in a new layered perovskite: (4-fluorophenethylammonium) $_2$ [CuCl $_4$], *J. Mater. Chem. C*, 2022, **10**, 5482–5488.
- 37 P.-F. Li, Y.-Y. Tang, Z.-X. Wang, H.-Y. Ye, Y.-M. You and R.-G. Xiong, Anomalous rotary polarization discovered in homochiral organic ferroelectrics, *Nat. Commun.*, 2016, **7**, 13635.
- 38 W. Y. Zhang, Y. Y. Tang, P. F. Li, P. P. Shi, W. Q. Liao, D. W. Fu, H. Y. Ye, Y. Zhang and R. G. Xiong, Precise Molecular Design of High- T_c 3D Organic-Inorganic Perovskite Ferroelectric: [MeHdabco]RbI $_3$ (MeHdabco = N-Methyl-1,4-diazoniabicyclo[2.2.2]octane), *J. Am. Chem. Soc.*, 2017, **139**, 10897–10902.
- 39 Y. Zhang, W. Q. Liao, D. W. Fu, H. Y. Ye, C. M. Liu, Z. N. Chen and R. G. Xiong, The First Organic-Inorganic Hybrid Luminescent Multiferroic: (Pyrrolidinium)MnBr $_3$, *Adv. Mater.*, 2015, **27**, 3942–3946.
- 40 Y. Zhang, W.-Q. Liao, D.-W. Fu, H.-Y. Ye, Z.-N. Chen and R.-G. Xiong, Highly Efficient Red-Light Emission in An Organic-Inorganic Hybrid Ferroelectric: (Pyrrolidinium)MnCl $_3$, *J. Am. Chem. Soc.*, 2015, **137**, 4928–4931.
- 41 Y. Wang, Z. Tang, C. Liu, J. Jiang, W. Liu, B. Zhang, K. Gao, H.-L. Cai and X. Wu, Room temperature ferroelectricity and blue photoluminescence in zero dimensional organic lead iodine perovskites, *J. Mater. Chem. C*, 2021, **9**, 223–227.
- 42 M. Rok, B. Zarychta, A. Bil, J. Trojan-Piegza, W. Medycki, A. Miniewicz, A. Piecha-Bisiorek, A. Ciżman and R. Jakubas, A multiaxial electrical switching in a one-dimensional organic-inorganic (pyrrolidinium) $_2$ Cd $_2$ I $_6$ ferroelectric and photoluminescent crystal, *J. Mater. Chem. C*, 2021, **9**, 7665–7676.
- 43 Z.-L. He, J.-H. Wei, J.-B. Luo, Z.-Z. Zhang and D.-B. Kuang, Reversible human-temperature-responsive luminescence switching in a Mn(II)-based metal halide, *J. Mater. Chem. C*, 2023, **11**, 1251–1257.
- 44 Q. Liu, H. Peng, J. C. Qi, Y. Z. Lu, S. J. Yang and W. Q. Liao, A photoluminescent chiral lead-free hybrid ferroelastic semiconductor with switchable second-harmonic generation, *Chem. Commun.*, 2023, **59**, 1793–1796.
- 45 Y. Wang, G. Lu, Y. Qiu, W. Sun, S. Qin, Y. Lin, B. Deng, D. Zhang and R. Yu, Synthesis and optical properties of novel apatite-type NaCa $_3$ Bi(PO $_4$) $_3$ F:Dy $^{3+}$ yellow-emitting fluorophosphate phosphors for white LEDs, *J. Rare Earths*, 2022, **40**, 1827–1836.
- 46 M. M. Kenisarin, High-temperature phase change materials for thermal energy storage, *Renewable Sustainable Energy Rev.*, 2010, **14**, 955–970.
- 47 X. Wang, X. Zhang, P. Tong, C. Yang, J. Si, T. Xiong, B. Dong, L. Xie, C. Pan, M. Wang, J. Lin, H. Chen, W. Yin, W. Song and Y. Sun, Latent heat thermal storage of solid-state phase transition in thermally stabilized hexagonal FeS, *Scr. Mater.*, 2023, **225**, 115166.
- 48 A. Caretta, R. Miranti, A. H. Arkenbout, A. O. Polyakov, A. Meetsma, R. Hidayat, M. O. Tjia, T. T. M. Palstra and P. H. M. van Loosdrecht, Thermochromic effects in a Jahn-Teller active layered hybrid system, *J. Phys.: Condens. Matter*, 2013, **25**, 505901.
- 49 R. Chen, H. Gu, Y. Han, J. Yin, G. Xing and B.-B. Cui, Broadband white-light emission from a novel two-dimensional metal halide assembled by Pb-Cl hendecahedrons, *J. Mater. Chem. C*, 2022, **10**, 9465–9470.
- 50 Z. Qi, Y. Chen, Y. Guo, X. Yang, F.-Q. Zhang, G. Zhou and X.-M. Zhang, Broadband white-light emission in a one-dimensional organic-inorganic hybrid cadmium chloride with face-sharing CdCl $_6$ octahedral chains, *J. Mater. Chem. C*, 2021, **9**, 88–94.
- 51 Z. Zhuang, C. Peng, G. Zhang, H. Yang, J. Yin and H. Fei, Intrinsic Broadband White-Light Emission from Ultra-stable, Cationic Lead Halide Layered Materials, *Angew. Chem., Int. Ed.*, 2017, **56**, 14411–14416.
- 52 S. Yang, Z. Lin, J. Wang, Y. Chen, Z. Liu, E. Yang, J. Zhang and Q. Ling, High Color Rendering Index White-Light Emission from UV-Driven LEDs Based on Single Luminescent Materials: Two-Dimensional Perovskites (C $_6$ H $_5$ C $_2$ H $_4$ NH $_3$) $_2$ PbBrxCl $_{4-x}$, *ACS Appl. Mater. Interfaces.*, 2018, **10**, 15980–15987.
- 53 G. Song, Z. Li, P. Gong, R. J. Xie and Z. Lin, Tunable White Light Emission in a Zero-Dimensional Organic-Inorganic Metal Halide Hybrid with Ultra-High Color Rendering Index, *Adv. Opt. Mater.*, 2021, **9**, 2002246.
- 54 G. Zhang, P. Dang, H. Xiao, H. Lian, S. Liang, L. Yang, Z. Cheng, G. Li and J. Lin, Antimony-Doped Lead-Free Zero-Dimensional Tin(IV)-Based Organic-Inorganic Metal Halide Hybrids with High Photoluminescence Quantum Yield and Remarkable Stability, *Adv. Opt. Mater.*, 2021, **9**, 2101637.
- 55 J. Q. Zhao, C. Sun, M. Yue, Y. Meng, X. M. Zhao, L. R. Zeng, G. Chen, C. Y. Yue and X. W. Lei, Lead chlorine cluster assembled one-dimensional halide with highly efficient broadband white-light emission, *Chem. Commun.*, 2021, **57**, 1218–1221.